



# Magnetic states and electronic properties of $\text{Sr}_4\text{V}_2\text{O}_6\text{Fe}_2\text{As}_2$ studied by DFT calculations



Thi Ly Mai<sup>a,\*</sup>, Vinh Hung Tran<sup>a</sup>

<sup>a</sup> W. Trzebiatowski Institute of Low Temperature and Structure Research, Polish Academy of Sciences, P.O. Box 1410, 50-422 Wrocław, Poland

## ARTICLE INFO

**Keywords:**  
Iron-based superconductors  
Electronic properties  
Inter-band scattering  
Nodal-lines structure

## ABSTRACT

In this work, we examine the magnetic stability of two incommensurate antiferromagnetic configurations and electronic band structures properties of  $\text{Sr}_4\text{V}_2\text{O}_6\text{Fe}_2\text{As}_2$  using first-principle density-functional-theory method. We show that the lowest total energy takes place in an incommensurate antiferromagnetic phase with the ordering wave vector  $q = (0.125, 0.125, 0)$  and ordered magnetic moment of  $1.25 \mu_B/\text{V}$ . Based on the total as well as partial density of states (DOS) data, it concludes that both Fe-3d and V-3d orbitals give a rise to DOS around Fermi level and lead to the occurrence of Van Hove singularity associated with electronic instability. A strong inter-band scattering in the incommensurate anti-ferromagnetic phases is proposed, since this behaviour is followed by a larger number of electronic bands crossing Fermi level as compared to those in nonmagnetic one. Electronic bands and Fermi surface data affirm multi-band structure superconductivity, where electron-like sheets of carriers with low Fermi velocities occur at the corner of the Brillouin zone and hole-like cylinders of carriers with high Fermi velocities situate around the  $\Gamma - Z$  line. Most importantly, our calculations predict the presence of both vertical and horizontal nodal lines, which seem to be distinct from usual feature of Fe-based superconductors with sole horizontal nodal lines.

## 1. Introduction

The Fe-based superconductivity in  $\text{Sr}_4\text{V}_2\text{O}_6\text{Fe}_2\text{As}_2$  crystallizing in the tetragonal structure with space group  $P4/nmm$  (No.129) first reported by Zhu et al. [1] has aroused intensive interest from several viewpoints: i) of magnetic ground state, due to the presence of magnetic Fe and V ions as well as ii) from the complex mechanism governing the coexistence of magnetism and superconductivity. From the overview of literature, it may be conjectured that the physical properties of  $\text{Sr}_4\text{V}_2\text{O}_6\text{Fe}_2\text{As}_2$  would differ from those of classic Fe-based superconductors in several aspects. At first,  $\text{Sr}_4\text{V}_2\text{O}_6\text{Fe}_2\text{As}_2$  with  $T_c = 37 \text{ K}$  and distance between neighbouring FeAs layers  $d_{\text{FeAs}-\text{FeAs}} \approx 15 \text{ \AA}$  evidently does not follow the relationship between  $T_c$  and  $d_{\text{FeAs}-\text{FeAs}}$  usually observed; e.g., for  $\text{LiFeAs}$  ( $d_{\text{FeAs}-\text{FeAs}} = 6.4 \text{ \AA}$ ,  $T_c = 18 \text{ K}$  [2]),  $\text{Ba}_{1-x}\text{K}_x\text{Fe}_2\text{As}_2$  ( $d_{\text{FeAs}-\text{FeAs}} = 6.5 \text{ \AA}$ ,  $T_c = 38 \text{ K}$  [3,4]) and  $\text{SmFeAsOF}$  ( $d_{\text{FeAs}-\text{FeAs}} = 8.7 \text{ \AA}$ ,  $T_c = 55 \text{ K}$  [5]). The second aspect is the additional complication in the superconductivity of  $\text{Sr}_4\text{V}_2\text{O}_6\text{Fe}_2\text{As}_2$  results from the presence of the V ions in the material. The V atoms not only, as a component of the perovskite  $\text{Sr}_4\text{V}_2\text{O}_6$  block, in addition to the contribution of  $\text{Fe}_2\text{As}_2$  layers, creates a new phonon spectrum, but as

magnetic ions, the V moments favour magnetic interactions and obviously would participate in the forming Copper pairs. In fact, at the hand of numerous experimental and theoretical efforts, the role of the V atoms in the superconducting  $\text{Sr}_4\text{V}_2\text{O}_6\text{Fe}_2\text{As}_2$  material was not clear-cut. In this connection it may be worthwhile to recall the following issues: i) Lee and Pickett [6] performing the Full-Potential Local Orbital (FPLO) calculations of electronic properties for nonmagnetic  $\text{Sr}_4\text{V}_2\text{O}_6\text{Fe}_2\text{As}_2$  phase, have postulated that this superconductor may possess different Fermi surfaces and character than those known up to now in Fe-based  $H T_c$  superconductors. Furthermore, the authors have suggested that in spite of a weak V–Fe coupling, the interaction along the zone boundary is sufficient strong to degrade the Fermi surface nesting. Interestingly, in the light of these considerations, the authors have argued that  $\text{Sr}_4\text{V}_2\text{O}_6\text{Fe}_2\text{As}_2$  represents a new paradigm for Fe-based superconductors, since the band structure does not satisfy the inter-band scattering condition. ii) However, the complex Fermi surfaces with no visible quasinegating features presented by Lee and Pickett have been deliberated by Mazin [7], who has interpreted this behaviour due to the V-3d electronic states. Taking into account only the Fe-3d bonds, the latter author has showed the bare susceptibility peak at  $(\pi, \pi)$ ,

\* Corresponding author.

E-mail address: [t.l.mai@intibs.pl](mailto:t.l.mai@intibs.pl) (T.L. Mai).

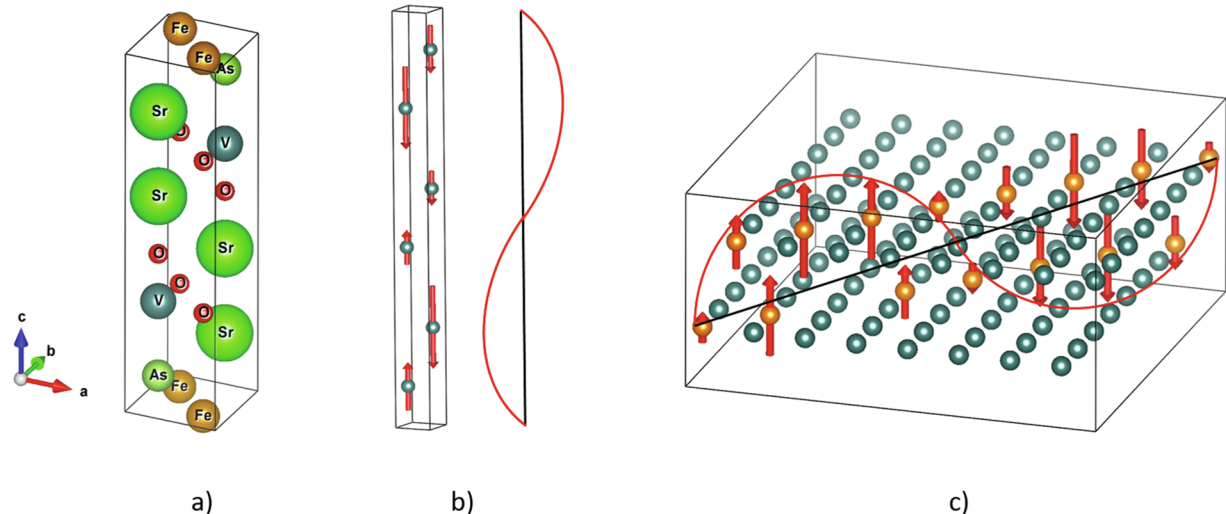


**Fig. 1.** a) The unit cell structure, and the incommensurate modulation of the antiferromagnetic spin structure of b) i-AF1, and c) i-AF2 configurations. (In Fig. b) and c), only V ions are presented in the super-cell.).

$0.4\pi$ ), which supports the quasi-nesting model. In addition, Mazin has suspected a strong Hubbard correlation of the V spins, that would move V-3d states away from the Fermi level. A similar conclusions have been derived from ARPES and LDA + U studies and put forward the importance of the inter-band scattering for the superconductivity in  $\text{Sr}_4\text{V}_2\text{O}_6\text{Fe}_2\text{As}_2$  [8]. iii) As regards possible magnetic states of  $\text{Sr}_4\text{V}_2\text{O}_6\text{Fe}_2\text{As}_2$ , there were several reports. Soon after the discovery of superconductivity in  $\text{Sr}_4\text{V}_2\text{O}_6\text{Fe}_2\text{As}_2$ , Shein and Ivanovski [9] have weigh up the energy of nonmagnetic and ferromagnetic states using FP-LAPW + Lo method. The authors have concluded a ferromagnetic configuration to be the stable state for  $\text{Sr}_4\text{V}_2\text{O}_6\text{Fe}_2\text{As}_2$ . iv) Another pursuits to determine magnetic states were conducted by Wang et al. [10] and Mazin [7]. These authors have considered manifold configurations of the V and Fe moments. Wang et al. and Mazin have accomplished the perception as regards the checkerboard AF configuration for the V moments but there is a constant risk of confusion between checker-board AF of Fe by Wang et al. and stripe AF of Fe in the Mazin calculations. The latter results are confined by Nakamura and Machida [11] and Tojo et al. [12]. It is necessary to reminisce that the V and Fe moments get large values of 1.9 and  $2.2 \mu_B$ , respectively, implying a localized character of the magnetism. v) We can recollect several experiments performed on  $\text{Sr}_4\text{V}_2\text{O}_6\text{Fe}_2\text{As}_2$ . The first is the  $^{57}\text{Fe}$  Mössbauer spectroscopy measurement [13], which announced nonmagnetic ordering at the Fe sites. The second and third experiments are the neutron-scattering [14] and polarized neutron diffraction [15], respectively. Surprisingly enough, the data of the cited neutron studies are not comparable with each other. On one hand, Tegel et al. have observed an incommensurate AF of the V moment with  $q = (0, 0, 0.306)$  (denoted in this work as i-AF1) [14], on the other hand, Hummel et al. have established a propagation vector  $q = (0.125, 0.125, 0)$  (denoted as i-AF2) [15]. After short consideration above, is clear that the lack of agreement among DFT calculations, among experimental data as well as

among theoretical and experimental results requires careful elucidation. Therefore, in this work, we examine electronic properties of  $\text{Sr}_4\text{V}_2\text{O}_6\text{Fe}_2\text{As}_2$ , possessing magnetic structures as determined by the neutron diffraction experiments.

The purpose of our studies was not only investigating in detail the difference in electronic properties of incommensurate structures with a propagating along the c-axis and on the ab-plane, but also aiming towards characterization of evolution of electronic properties upon the change caused by the V moment ordering. Accordingly, we also re-calculated electronic structure for nonmagnetic (NM) state. To the best of our knowledge, there was no DFT study on these incommensurate AF structures. Therefore, this work sheds new light on the electronic properties of  $\text{Sr}_4\text{V}_2\text{O}_6\text{Fe}_2\text{As}_2$  by DFT investigating the incommensurate AF configurations, which were established by neutron diffraction experiments.

## 2. Computational approach

We investigated the stability of antiferromagnetic configurations and electronic band properties of  $\text{Sr}_4\text{V}_2\text{O}_6\text{Fe}_2\text{As}_2$  according to the following steps: (i) we optimized the lattice parameters and atomic positions in  $\text{Sr}_4\text{V}_2\text{O}_6\text{Fe}_2\text{As}_2$ , (ii) we performed self-consistent calculations of the charge densities for two incommensurate AF configurations with magnetic ordering wave vectors  $q_1 = (0, 0, 0.306)$  and  $q_2 = (0.125, 0.125, 0)$ , which are respectively illustrated in Fig. 1 b) and c),(iii) we determined the band structure properties, i.e., total densities of states (TDOS), interstitial density of states (IDOS), partial densities of states (PDOS) of the V-3d and Fe-3d electrons, electronic band structures (EBS) and Fermi surfaces (FS). The crystal structure relaxation (step i) was done by employing the Vienna ab initio simulation package (VASP) within the projector augmented wave (PAW) method [16]. The plane waves with a cut-off energy of 400 eV were applied for the basic sets.

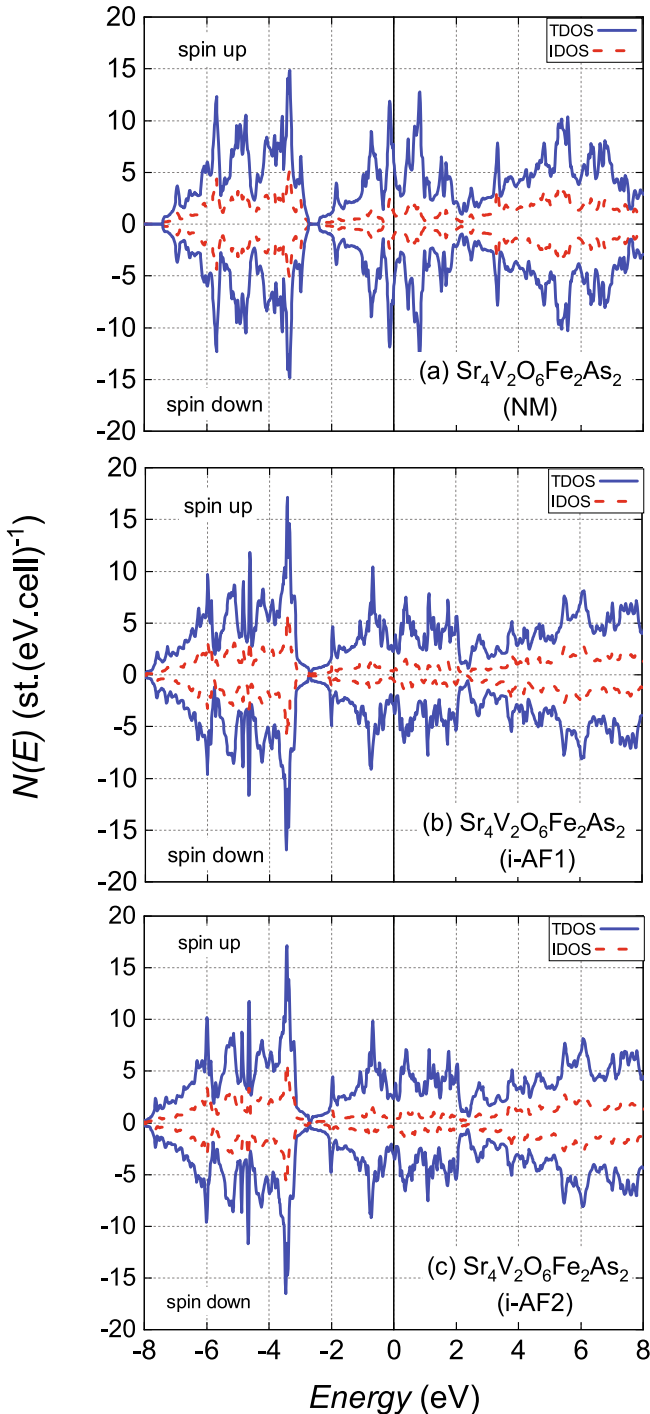


**Fig. 2.** The total (solid line) and interstitial (dashed line) density of states of  $\text{Sr}_4\text{V}_2\text{O}_6\text{Fe}_2\text{As}_2$  in the a) NM, b) i-AF1, and c) i-AF2 configurations in the energy range (-8 ÷ 8 eV).

**Table 1**

Calculated total energies  $E$  in i-AF1 and i-AF2  $\text{Sr}_4\text{V}_2\text{O}_6\text{Fe}_2\text{As}_2$  phases using ELK. The values of  $E$  are given relatively to the energy of the NM phase.

Mag. struct.	$\Delta E$ (meV)
i-AF1	-51.7
i-AF2	-129.5

For the Brillouin zone, we chose  $20 \times 20 \times 5$  Monkhorst–Pack grid including 198 k-points. As input parameters, we took our crystallographic experiment results [17] with the following parameters:  $a = b = 3.9318 \text{ \AA}$ ,  $c = 15.6910 \text{ \AA}$  and the atomic positions  $z_{\text{Sr}1} = 0.1903$ ,  $z_{\text{Sr}2} = 0.4145$ ,  $z_V = 0.3081$ ,  $z_{\text{O}1} = 0.2922$ ,  $z_{\text{O}2} = 0.4318$ ,  $z_{\text{Fe}} = 0.0000$ , and  $z_{\text{As}} = 0.0909$ . The optimized process was completed when the different energy was reached at  $5.10^{-5} \text{ eV}$  and the force was less than  $0.01 \text{ eV}/\text{\AA}$ . After the geometry relaxation, the optimized unit cell volume is reduced by 14 % and the atomic coordinate parameters are slightly changed. In details, the relaxed crystallographic parameters were found as follow:  $a = b = 3.7937 \text{ \AA}$ ,  $c = 14.5016 \text{ \AA}$  and  $z_{\text{Sr}1} = 0.1768$ ,  $z_{\text{Sr}2} = 0.4121$ ,  $z_V = 0.2944$ ,  $z_{\text{O}1} = 0.2876$ ,  $z_{\text{O}2} = 0.4268$ ,  $z_{\text{Fe}} = 0.0$ ,  $z_{\text{As}} = 0.0864$ . The fully relativistic self-consistent (step ii) and electronic structures properties (step iii) of  $\text{Sr}_4\text{V}_2\text{O}_6\text{Fe}_2\text{As}_2$  system were calculated employing all-electron full-potential linearized augmented-plane wave (LAPW) method, implemented in the ELK code [18]. We used a dense mesh of  $16 \times 16 \times 4$  with 72, 144, and 544 k-points in NM, i-AF1, and i-AF2 phases for the Brillouin zone, respectively. While the Fermi surface calculations were carried out with  $60 \times 60 \times 60$  k-point mesh. Besides, the high-symmetry line  $Z(0, 0, 0.5) - R(0, 0.5, 0.5) - X(0, 0.5, 0) - M(0.5, 0.5, 0) - \Gamma(0, 0, 0) - Z(0, 0, 0.5) - A(0.5, 0.5, 0.5) - M(0.5, 0.5, 0) - R(0, 0.5, 0.5) - A(0.5, 0.5, 0.5)$  was chosen for electronic band structure study. The self-consistent calculation was finished when an absolute change in total energy reaches a converged value of 1 meV. The muffin-tin radii of all atoms were gotten as:  $R_{\text{Sr}} = 2.600$  (a.u.),  $R_V = 2.025$  (a.u.),  $R_O = 1.152$  (a.u.),  $R_{\text{Fe}} = R_{\text{As}} = 2.123$  (a.u.).

The generalized gradient approximations (PBEsol-GGA) [19], the spin-orbit interaction as well as spin-polarized effect were additionally applied for the all calculations in both nonmagnetic and magnetic phases. To analyse Fermi surfaces in a more detail, we determined several FS section areas cross directions (001), (110), (-110) and (010) using the Fermisurfer software [20].

In addition, the DOS for two magnetic configurations also were calculated using the LDA + U method as implemented in the Vienna ab initio simulation package (VASP), where the Hubbard U correction and Hunds coupling J were involved. The Brillouin zone was used as  $16 \times 16 \times 4$  Monkhorst-Pack grid including 133 k-points.

### 3. Results

The total and interstitial density of states of  $\text{Sr}_4\text{V}_2\text{O}_6\text{Fe}_2\text{As}_2$  in nonmagnetic (NM) and two incommensurate antiferromagnetic (i-AF1, i-AF2) states are depicted in Fig. 2. Apparently, TDOS calculated for

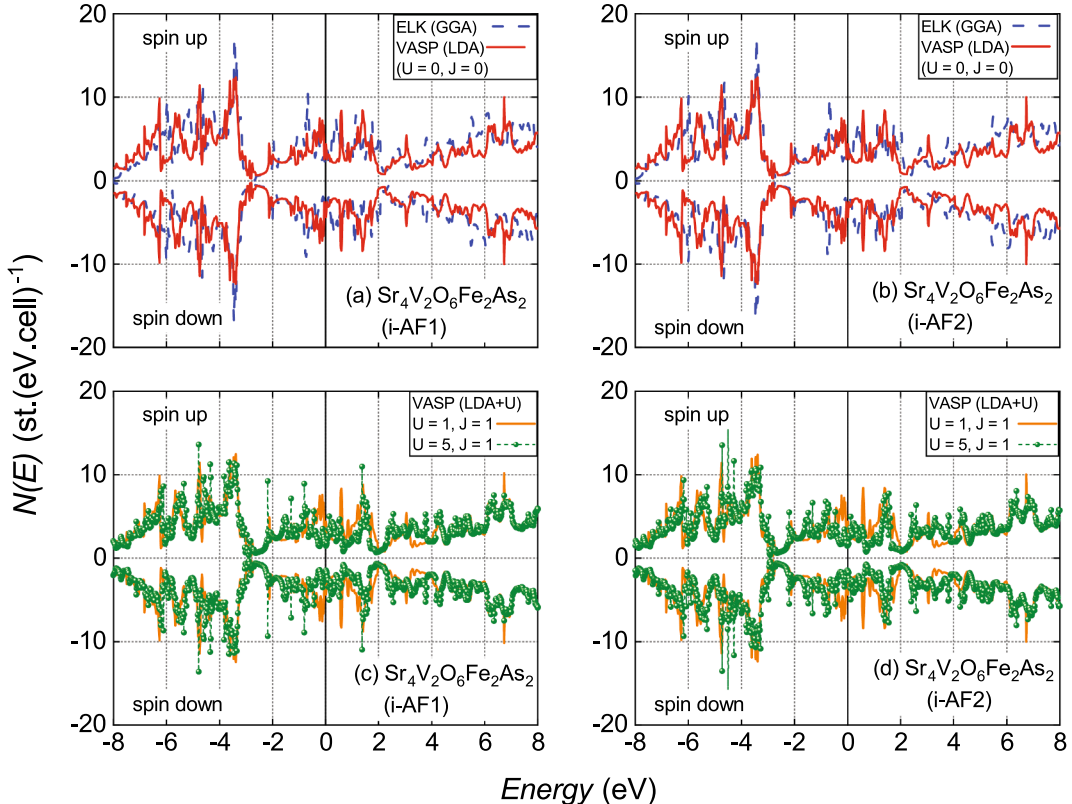


**Fig. 3.** The total density of states of i-AF1 and i-AF2  $\text{Sr}_4\text{V}_2\text{O}_6\text{Fe}_2\text{As}_2$  in the case of a), b)  $(U, J) = (0, 0)$  using ELK and VASP, and c), d)  $(U, J) = (1, 1)$  eV,  $(U, J) = (5, 1)$  eV using VASP.

**Table 2**

The density of states at Fermi level, magnetic moment of V, and total energy in several cases of  $(U, J)$  using ELK and VASP in i-AF1 and i-AF2  $\text{Sr}_4\text{V}_2\text{O}_6\text{Fe}_2\text{As}_2$  phases.

Code	$(U, J)$ eV	N( $E_F$ ) st/(eV.cell)		Moment of V ( $\mu_B$ )		Total energy (eV)	
		i-AF1	i-AF2	i-AF1	i-AF2	i-AF1	i-AF2
ELK (GGA)	(0, 0)	5.654	5.653	1.251	1.249	-812.401	-812.401
VASP (LDA)	(0, 0)	8.420	8.420	0.01	0.01	-122.037	-122.037
	(1, 1)	8.420	8.420	0.01	0.01	-122.037	-122.037
	(3, 1)	8.599	8.600	1.237	1.237	-117.782	-117.782
	(5, 1)	8.481	8.455	1.500	1.518	-114.081	-114.071

these configurations are similar to another in the energy range  $-8 \div -3$  eV. In fact, the TDOS below  $-3$  eV are build up by the s and p orbitals, and hence they have not thing to do with the magnetic order. The discernible differences in TDOS between these phases crop up in the energy range  $-2 \div 8$  eV. For the NM state, the Fermi level ( $E_F$ ) lies at a steep DOS hill, whereas for both i-AF1 and i-AF2 the position of  $E_F$  is just located at a valley of two DOS peaks. This situation causes that the DOS at the  $E_F$  level take different values, i.e., 12.054 st/(eV.cell) for the NM, and only 5.654 st/(eV.cell) or 5.653 st/(eV.cell) for i-AF1 and i-AF2 phases.

Furthermore, we observe that the DOS for NM with two peaks below  $E_F$  manifest a more complicated structure as compared to one-peak structure in the case of i-AF. Besides, the total energies of the two i-AF configurations relatively to the energy of the NM phase, given in TABLE 1, reveal that the i-AF2 is considerably more stable than the i-AF1, being about 78 meV lower in the total energy  $E$ . It may be recalled that our data for NM are in good agreement with those reported by Lee and Pickett [6]. Two physical quantities: electronic specific heat coefficient (Sommerfeld coefficient –  $\gamma_{\text{theo}}$ ) theoretically presenting a sum of electron, phonon or additional boson contributions, and densities of states

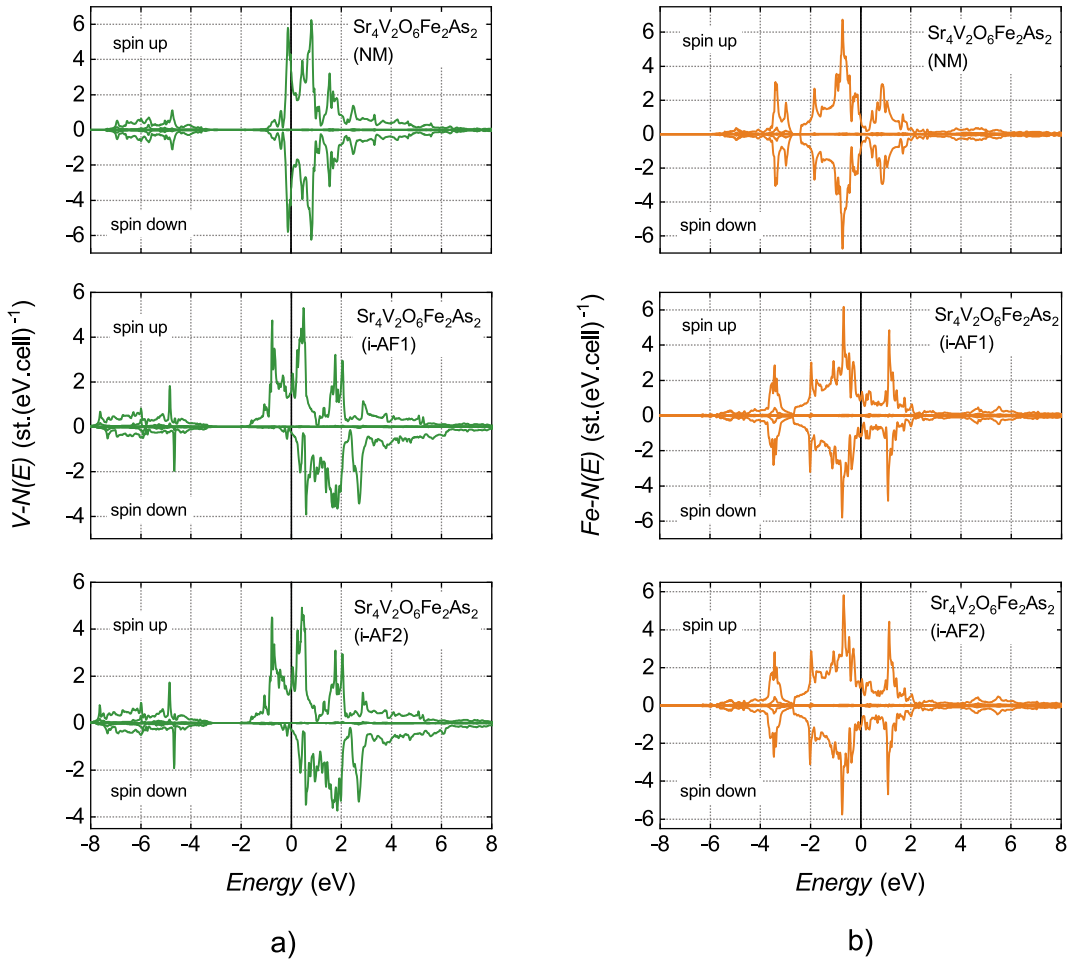


**Fig. 4.** The partial density of states of a) V and b) Fe atoms in NM, i-AF1, and i-AF2 of  $\text{Sr}_4\text{V}_2\text{O}_6\text{Fe}_2\text{As}_2$  in the energy range ( $-8 \div 8$  eV).

at the Fermi level  $N(E_F)$  are associated themselves by the relation:

$$\gamma_{\text{theo}} = \frac{2}{3} \pi^2 k_B^2 N_A N(E_F), \quad (1)$$

where  $k_B$  is the Boltzmann constant, and  $N_A$  is Avogadro's number. Putting the theoretical  $N(E_F)$  values of 6.03 st/(eV.mol) for NM and 2.83 st/(eV.mol) for i-AF phases, respectively, into the Eq. 1, we obtained appropriately theoretical  $\gamma_{\text{theo}}$  values of 14.19 and 6.66 mJ/molK<sup>2</sup>, corresponding to the total electron-phonon coupling and electronic correlations parameter  $\lambda_t$  of 1.36 and 4.03, if using the experimental  $\gamma_{\text{exp}} = 33.5$  mJ/molK<sup>2</sup> [17] and taking into account the relation:  $\lambda_t = \frac{\gamma_{\text{exp}}}{\gamma_{\text{theo}}} - 1$ . The pronounced difference in the  $\lambda_t$ -values implies that the magnetic interactions between the V moments would affect the coupling forming the Cooper pairs.

In Fig. 3 a) and b) we present results of DOS obtained within the GGA (dashed line) and LDA (solid line) approximations for i-AF1 and i-

AF2 with  $U = 0$  and  $J = 0$ . In TABLE 2, we summarize the calculated parameters of  $\text{Sr}_4\text{V}_2\text{O}_6\text{Fe}_2\text{As}_2$  in two AF configurations. Our results show that the DOS structures resulting from two approximations are comparable. At energies below  $-3$  eV there is peak structure corresponding the contributions of s and p states. At higher energies around  $E_F$  there are four peaks which are mainly due to the V and Fe d states. However, these peaks from GGA and LDA are little shifted in respect to each other. We can observe that the LDA approximation yields a narrower dispersion of bands, and then leads to higher densities of states at  $E_F$ . The influence of the Hubbard U correction on the DOS of  $\text{Sr}_4\text{V}_2\text{O}_6\text{Fe}_2\text{As}_2$  can be assessed throughout an inspection of Fig. 3 c) and d) for i-AF1 and i-AF2, respectively. Selected data, i.e., only for  $U = 1$  and 5 eV, manifest usual behaviour in the U-dependence of DOS. An increase of U values causes subtle changes in DOS structure near  $E_F$ . The DOS peaks just below  $E_F$  are slightly lower but DOS peaks above  $E_F$  move up to higher energies. So, there is larger splitting of bands. We may notice that the magnetic ordered moment of the V ions are

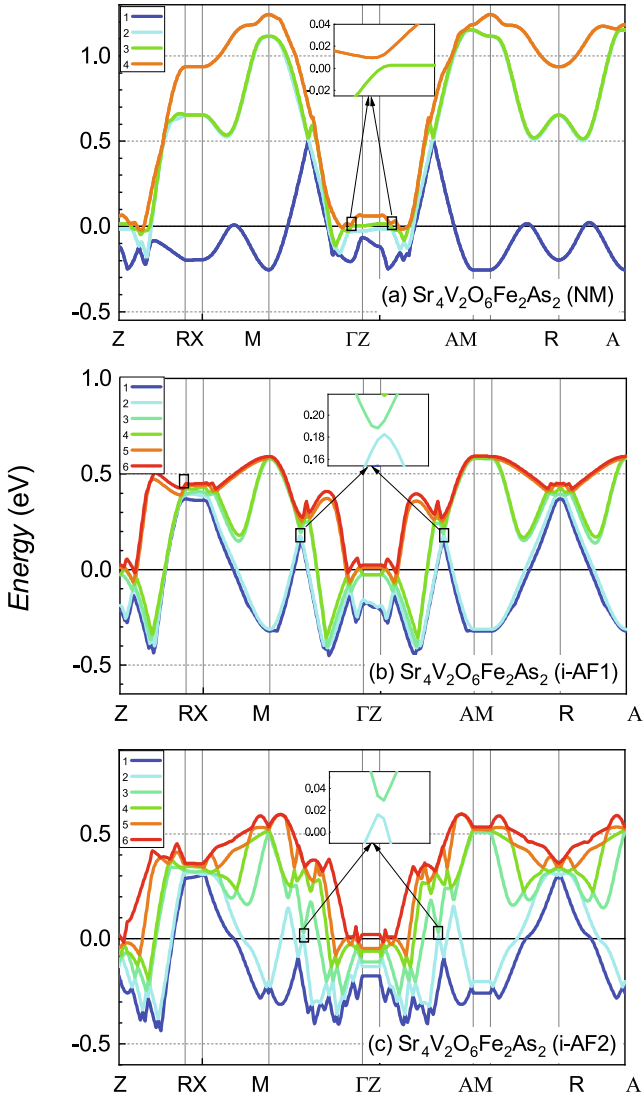


**Fig. 5.** Electronic band structures of  $\text{Sr}_4\text{V}_2\text{O}_6\text{Fe}_2\text{As}_2$  in a) NM, b) i-AF1, and c) i-AF2 configurations. The enlarged parts of bands highlight the nodal line state.

enhanced but they are still lower than those reported in literature. In spite of the change in DOS structures, the  $N(E_F)$  seem to be preserved and there is absence of band gap. Therefore, our results suggest that in the case of magnetic i-AF, the Hubbard U correction does not influence significantly the electronic properties of  $\text{Sr}_4\text{V}_2\text{O}_6\text{Fe}_2\text{As}_2$ .

To examine the role of the V and Fe atoms in the evolution of magnetic states of  $\text{Sr}_4\text{V}_2\text{O}_6\text{Fe}_2\text{As}_2$ , we calculated the partial densities of states of these atoms. The obtained PDOS are given in Fig. 4a for V and Fig. 4b for Fe, respectively. An inspection of the data provides a few interesting findings as it follows: i) The lack of the spin polarization in the Fe-3d PDOS, indicating the absence of magnetic moment at the Fe sites in all considered phases. ii) The PDOS of the V- and Fe-3d orbitals

in NM phase are very well resolved; As a result the DOS peaks located at  $\sim -0.8$  and  $\sim 0.1$  eV are derived from the Fe and V atoms, respectively. iii) The PDOS structures of the V-3d orbitals in i-AF1 and i-AF2 are similar. The PDOS extend in the energy range from  $-2$  to  $6$  eV exhibit a pronounced spin polarization. The finding implies that the AF-order originates only from the V moments. iv) Large exchange between the V moments exposed by the spin polarization calculations provides magnetic moment of  $\sim 1.25 \mu_B/\text{V}$ . Few eventual reasons for the lowering magnetic moment compared to those previously reported will be considered in the next section. v) The PDOS of the V-3d and Fe-3d in i-AF phases locate at similar energy position of  $\sim -0.8$  eV. This suggests possible hybridization between V-3d and Fe-3d orbitals. Consequently, not only Fe-3d but also V-3d electrons would participate in the creating Cooper pairs. The electronic band structures of  $\text{Sr}_4\text{V}_2\text{O}_6\text{Fe}_2\text{As}_2$  near  $E_F$  are shown in Fig. 5. We observe four bands crossing  $E_F$  in the NM phase, while as many as six bands passing  $E_F$  in the i-AF phases. The bands are numbered accordingly from 1 to 4, and from 1 to 6. Apparently, the contribution of peculiar electronic band to the densities of states at  $E_F$  is different. In the NM phase, this contribution is predominantly due to the band 1 while in i-AF phases by the bands 1 and 2. It must be pointed that the width of band 1 in the NM phase amounts to about 0.8 eV, relatively narrower than the band-width of band 2–4 of  $\sim 1.2$  eV. In the case of i-AF phases, the width of all bands is comparable and amounts to about 0.8 eV. It is remarkable that in i-AF1 the bands of pairs 1 and 2, 3 and 4, and 5 and 6 weakly de-merge. Contrariwise, these bands in i-AF2 are greatly split, surely due to stronger magnetic interactions. It can be presumed that the larger number of bands crossing  $E_F$  in both i-AF phases compared to that of NM exhorts appreciably inter-band scattering in the i-AF phases, which would affect the superconductivity. This observation connotes the existence of a relationship between superconductivity and magnetism. An another striking feature of the electronic bands is the possibility of the formation of Dirac nodal lines around the Fermi level. As an illustration, we show in Fig. 5 enlarged excerpt of selected bands nearby  $E_F$ . In all likelihood, along the  $k$ -path M- $\Gamma$  and as well as along the path Z-A, at least, two bands, i.e., bands 3 and 4 in NM, likewise bands 2 and 3 in i-AF configurations, cross together in the case of without Spin-Orbit Coupling (SOC) but they form a small SOC-induced gap of less than 13 meV. Furthermore, a closer examination of the EBS reveals numerous band-crossing points, which occur along the  $k$ -paths R-X, X-M, A-M and M-R. Obviously, we can realize that the latter node points lie on horizontal nodal lines while the other nodal points e.g., as shown in enlarged insets of Fig. 5 prevail vertical ones. In Fig. 6, we present projected V-3d and Fe-3d orbitals. At first glance, the contribution of V-3d and Fe-3d orbitals to bands is similar, but at closely examining, one sees that the thickness of the Fe-3d bands is slightly larger. This means that the weight of Fe-3d states would be larger.

The 3D as well as 2D FS topologies of  $\text{Sr}_4\text{V}_2\text{O}_6\text{Fe}_2\text{As}_2$  in non-magnetic and two different incommensurate AF configurations (i-AF1, i-AF2) are presented in Fig. 7. In NM phase, the FS consists of three hole-type cylinders along the  $\Gamma-Z$  direction and one unclosed electron-type sheet around the  $M$  point with a large dispersion, which is quite alike with FS results obtained by Hummel et al. in the LDA-GGA approximation [15]. Completely different FS topologies to that of NM are found in both i-AF1 (Fig. 7 b) and i-AF2 (Fig. 7c) phases. Both bands

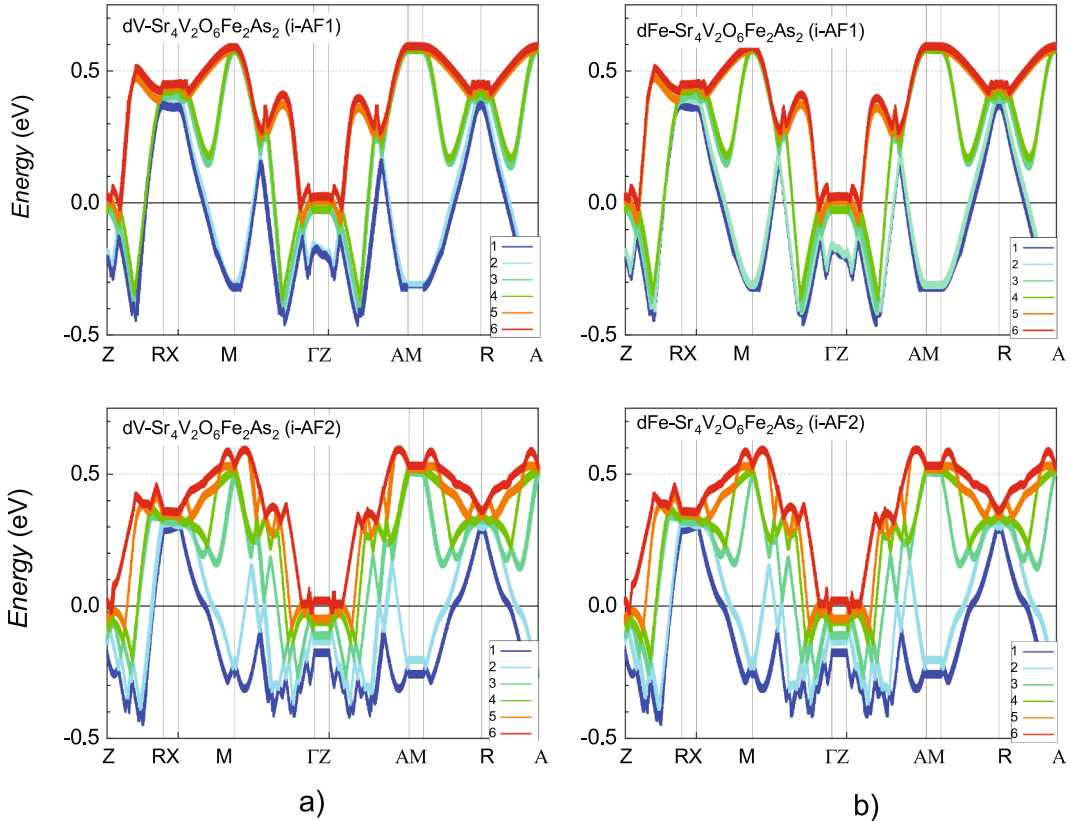


**Fig. 6.** The distribution of a) V-3d and b) Fe-3d orbitals in electronic band structures of  $\text{Sr}_4\text{V}_2\text{O}_6\text{Fe}_2\text{As}_2$  in i-AF1 and i-AF2 configurations.

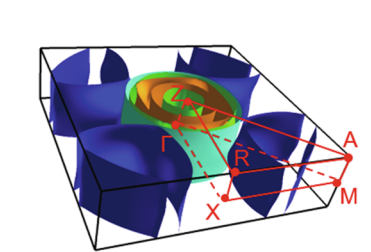
1 and 2 of i-AF1 form electron-type sheets at the corner and hole-type square pillars around the  $\Gamma - Z$  line. The bands 3 and 4 respond for large hole-type cylinders, very closely situated. Moreover, the band 4 exhibits moreover small sheets at the center. Each of the bands 5 and 6 contributes to two small hole-type cylinders close to the  $\Gamma - Z$  line. Note that the FS of band 6 take place between those of band 5. The robust topological property of i-AF1 is different to that in i-AF2, where the ab-plane isotropy no longer exists. In a detail, the band 1 of i-AF2 exhibits two electron-type sheets at two opposite sites of the BZ corners, and does not show any FS sheet at the two remaining corners. The band 2 builds up small FS sheet at the BZ corners and large ellipse-shaped hole-type cylinder around the  $\Gamma - Z$  line. The band 4 characterizes by only one hole-type square pillar. The bands 4, 5 and 6 create complex FS, which involve ellipse-shaped hole-type cylinder and small hole-type cylinder from the band 4, hole-type cylinder and several small closed sheets from the band 5 and finally two tiny hole-type closed sheets from the band 6. Based on the comparison of FS between those of i-AF1 and i-AF2, we believe that the change in FS topologies from 2D-quasi topology in i-AF1 to 3D topology in i-AF2 certainly corresponds to change of the ordering wave vectors, i.e. from  $(0, 0, k_z)$  to  $(k_x, k_y, 0)$ .

In Fig's 8–10, we show FS cutting cross several directions together

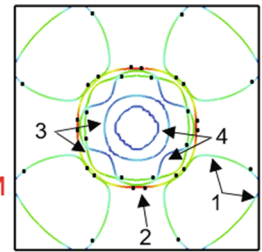
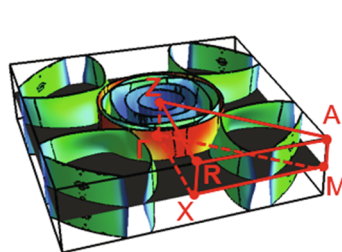
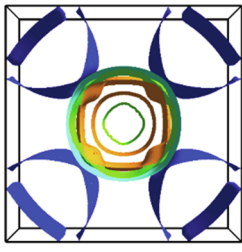
with Fermi velocities and nodal lines. A most important insight from the study is that the FS do exhibit both horizontal (perpendicular to the tetragonal c axis) and vertical nodal (parallel to the tetragonal c axis) lines and also different Fermi velocities of charge carriers depending on which FS areas they are. With regard to the nodal lines, we see that the FS of NM and i-AF2 phases have one horizontal line at  $k_z = 0$  in all FS sheets, whereas the FS sheets of i-AF1 phase have horizontal lines which come about at  $k_z = 0.15$  for bands 1, 3, 5 and at  $k_z = 0.35$  for bands 2, 4, and 6. The change in the Fermi velocities from low to high values is drawn according to the colour bar from blue to red. In all three studied phases, it is found that the hole carries on the bands 2, 3 and 4 exhibit high Fermi velocities. This behaviour is in opposite to the electron carries on the bands 1 and 6 with low Fermi velocities. In this connection, it should be pointed out that some FS sheets having low and high Fermi velocities meet at special lines echoing possibility of nodal structure superconductivity.

#### 4. Discussion and conclusions

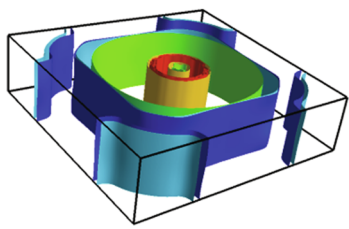
We have investigated the electronic band structures properties of the high- $T_c$  superconductor  $\text{Sr}_4\text{V}_2\text{O}_6\text{Fe}_2\text{As}_2$  in nonmagnetic as well as



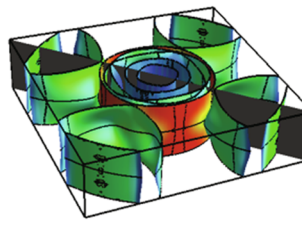
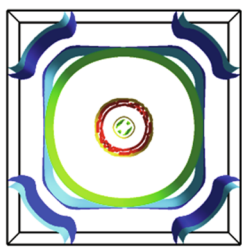
(a) NM



(001)

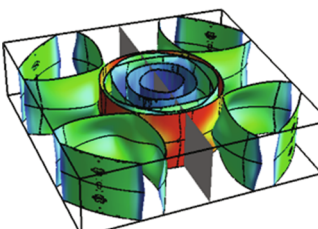


(b) i-AF1



(110)

(c) i-AF2



(100)

**Fig. 7.** Fermi surfaces in 3D topology and the 2D-quasi as seen perpendicularly to 001 plane of  $\text{Sr}_4\text{V}_2\text{O}_6\text{Fe}_2\text{As}_2$  in both a) NM and b) i-AF1, and c) i-AF2 phases. Color codes of FS are the same as presented for the electronic bands in Fig. 5.

incommensurate anti-ferromagnetic states with  $q = (0, 0, 0.306)$  (i-AF1) and  $q = (0.125, 0.125, 0)$  (i-AF2). Our calculations divulge that the i-AF2 is the most stable magnetic configuration amongst considered cases. Only the  $\text{V}^{3+}$  carry magnetic moments of  $1.25 \mu_B$  and obviously, nonmagnetic state of the Fe atoms was obtained in our calculations. Basically, our data disagree with those in previous published studies [11,12], not only by non-magnetic ground state of Fe but also by magnitude of magnetic moments of V. A lowering of magnetic moment might naively be expected if there exists an unquenched large orbital moment  $\mu_L$ . In the considered case,  $\mu_L$  measuring up  $0.75 \mu_B$  presumably signs oppositely to the spin moment of  $\mu_S = 2 \mu_B$ . This situation happens in systems with strong spin-orbit interactions and weak JahnTeller distortion [21]. On the other hand, spin-fluctuation effect

**Fig. 8.** 3D topology of Fermi surfaces, Fermi velocities and FS cuts in several directions of NM  $\text{Sr}_4\text{V}_2\text{O}_6\text{Fe}_2\text{As}_2$ . The black lines in 3D topology show horizontal and vertical nodal lines while black dots in the 001 cut show vertical nodal lines. The number stands for the label of bands as indicated in Fig. 5. The colour bar scale from blue to red corresponds to the Fermi velocities from low to high magnitude, respectively.

could be suitable mechanism to explain the reduction of the moment [22]. This scenario seems to be plausible in itinerant electronic systems, where the magnetic spins forcefully hybridise with conduction electrons. Unfortunately, this is not the case for  $\text{Sr}_4\text{V}_2\text{O}_6\text{Fe}_2\text{As}_2$  in which the V atoms inside the perovskite frame are surrounded by O atoms, and the V 3d orbitals are found to be in a Mott insulating state [23]. The DFT calculations within the GGA and LDA approximations yield comparable results. The Hubbard U correction results in larger magnetic moments of V but seems to not influence significantly electronic structures. The

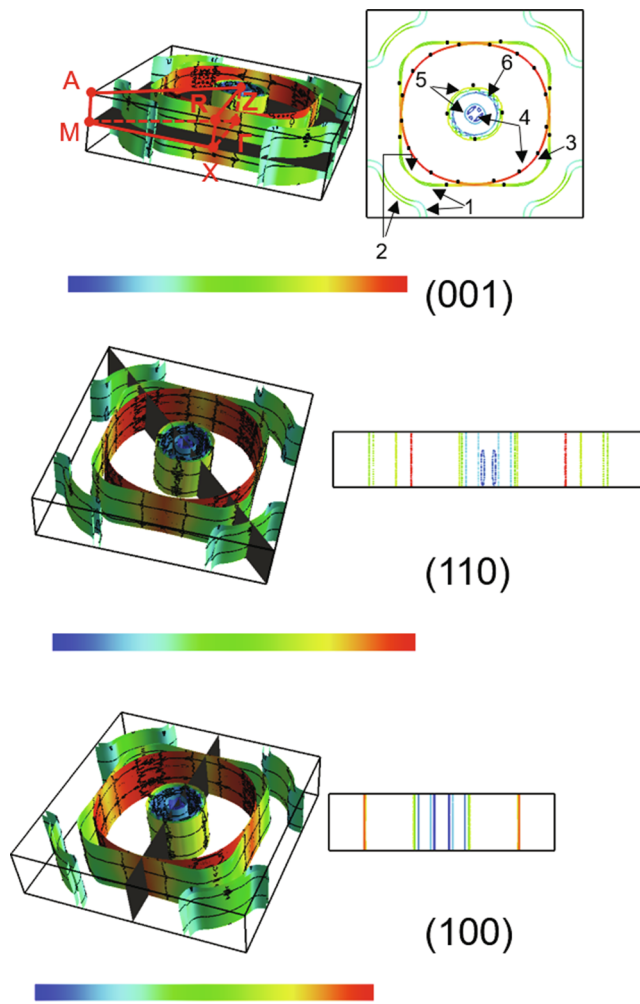


**Fig. 9.** 3D topology of Fermi surfaces, Fermi velocities and FS cuts in several directions of i-AF1  $\text{Sr}_4\text{V}_2\text{O}_6\text{Fe}_2\text{As}_2$ . The black lines in 3D topology show horizontal and vertical nodal lines while black dots in the 001 cut show vertical nodal lines. The number stands for the label of bands as indicated in Fig. 5. The colour bar scale from blue to red corresponds to the Fermi velocities from low to high magnitude, respectively.

present theoretical study is the first work reporting on the existence of vertical and horizontal nodal lines in  $\text{Sr}_4\text{V}_2\text{O}_6\text{Fe}_2\text{As}_2$ . Previously, the occurrence of nodal line states in other superconducting Fe-based materials has been documented by different measurement techniques, like thermal conductivity, penetration depth, nuclear magnetic resonance, scanning tunnelling microscope (STM), ARPES, and magnetic penetration depth measurements [24–31]. Remarkably, the horizontal nodal states usually occur in Fe-based superconductors with strong  $d_{3z^2-r^2}$  orbital characters [28,32,33]. At the same time, the realisation of d-wave pairing symmetry with the  $d_{x^2-y^2}$  orbital character assisting vertical line nodes as in the SC cuprates [34] might be excluded. Therefore, we hope that the prediction of vertical and horizontal nodal lines in  $\text{Sr}_4\text{V}_2\text{O}_6\text{Fe}_2\text{As}_2$  calls for future experimental efforts.

In conclusion, we are of the opinion that besides its interest as the coexistence of superconductivity and complex AF ordering,  $\text{Sr}_4\text{V}_2\text{O}_6\text{Fe}_2\text{As}_2$  may offer new subject to explore the physics of

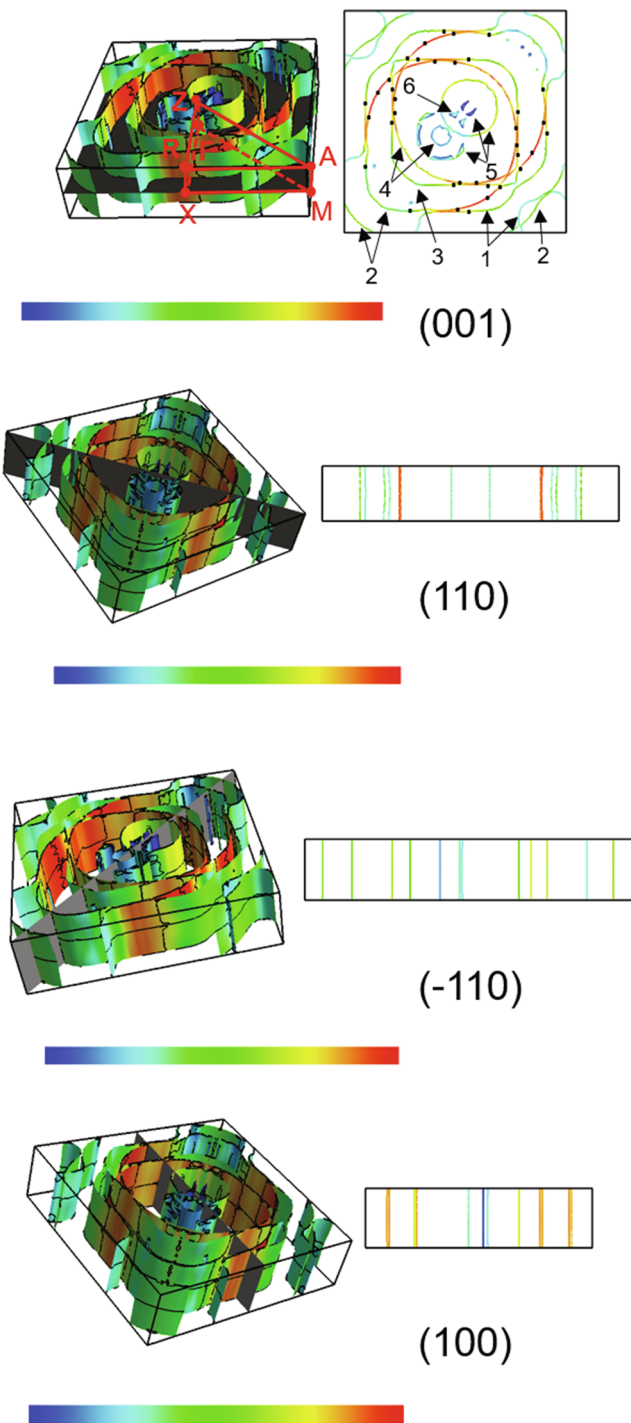


**Fig. 10.** 3D topology of Fermi surfaces, Fermi velocities and FS cuts in several directions of i-AF2  $\text{Sr}_4\text{V}_2\text{O}_6\text{Fe}_2\text{As}_2$ . The black lines in 3D topology show horizontal and vertical nodal lines while black dots in the 001 cut show vertical nodal lines. The number stands for the label of bands as indicated in Fig. 5. The colour bar scale from blue to red corresponds to the Fermi velocities from low to high magnitude, respectively.

topological superconductors.

### Declaration of Competing Interest

The authors declare that they have no known competing financial interests or personal relationships that could have appeared to influence the work reported in this paper.

### Acknowledgements

The financial support by the National Science Centre of Poland under the Grant No. 2016/21/B/ST3/01366 is gratefully acknowledged.

### References

- [1] X. Zhu, F. Han, G. Mu, P. Cheng, B. Shen, B. Zeng, H.-H. Wen, 79, 220512 (2009), 0904.1732, URL:<https://ui.adsabs.harvard.edu/abs/2009PhRvB.79v0512Z>.
- [2] J.H. Tapp, Z. Tang, B. Lv, K. Sasmal, B. Lorenz, P.C.W. Chu, A.M. Guloy, Phys. Rev. B 78 (2008), <https://doi.org/10.1103/PhysRevB.78.060505> ISSN 1550-235X.
- [3] M. Rotter, M. Tegel, D. Johrendt, Phys. Rev. Lett. 101 (2008) 107006, , <https://doi.org/10.1103/PhysRevLett.101.107006>.
- [4] K. Sasmal, B. Lv, B. Lorenz, A.M. Guloy, F. Chen, Y.-Y. Xue, C.-W. Chu, Phys. Rev. Lett. 101 (2008) 107007, , <https://doi.org/10.1103/PhysRevLett.101.107007>.
- [5] A. Srivastava, A. Pal, S. Singh, C. Shekhar, H. Singh, V. Awana, O. Srivastava, AIP Adv. 3 (2013), <https://doi.org/10.1063/1.4821335>.
- [6] K.-W. Lee, W.E. Pickett, Europhys. Lett. 89 (2010) 57008URL: <https://doi.org/10.1209%2F0295-5075%2F89%2F57008>
- [7] I.I. Mazin, Phys. Rev. B 81 (2010) 020507, , <https://doi.org/10.1103/PhysRevB.81.020507>.
- [8] T. Qian, N. Xu, Y.B. Shi, K. Nakayama, P. Richard, T. Kawahara, T. Sato, T. Takahashi, M. Neupane, Y.M. Xu, et al., arXiv e-prints arXiv:1008.4905 (2010), 1008.4905.
- [9] I.R. Shein, A.L. Ivanovskii, J. Supercond. Nov. Magn 22 (2009) 613, <https://doi.org/10.1007/s10948-009-0489-2> ISSN 1557-1947.
- [10] G. Wang, M. Zhang, L. Zheng, Z. Yang, Phys. Rev. B 80 (2009) 184501, , <https://doi.org/10.1103/PhysRevB.80.184501>.
- [11] H. Nakamura, M. Machida, Phys. Rev. B 82 (2010) 094503, <https://doi.org/10.1103/PhysRevB.82.094503>.
- [12] Y. Tojo, T. Shibusawa, T. Nakamura, K. Shoji, H. Fujioka, M. Matoba, S. Yasui, M. Itoh, S. Iimura, H. Hiramatsu, et al., J. Condens. Matter Phys. 31 (2019) 115801URL: <https://doi.org/10.1088%2F1361-648x%2Faaf7e0>.
- [13] G.-H. Cao, Z. Ma, C. Wang, Y. Sun, J. Bao, S. Jiang, Y. Luo, C. Feng, Y. Zhou, Z. Xie, 82 (2010) 104518, 1007.3980, URL: <https://ui.adsabs.harvard.edu/abs/2010PhRvB..82j4518C>.
- [14] M. Tegel, F. Hummel, Y. Su, T. Chatterji, M. Brunelli, D. Johrendt, EPL (Europhysics Letters) 89 (2010) 37006URL: <https://doi.org/10.1209%2F0295-5075%2F89%2F57008>.
- [15] F. Hummel, Y. Su, A. Senyshyn, D. Johrendt, 88 (2013) 144517. 1307.2138, URL: <https://ui.adsabs.harvard.edu/abs/2013PhRvB.88n4517H>.
- [16] G. Kresse, J. Hafner, Phys. Rev. B 47 (1993) 558, <https://doi.org/10.1103/PhysRevB.47.558>.
- [17] V.H. Tran et al. (To be published, 2020).
- [18] J.K. Dewhurst et al. Elk code, version 5.2.14 (2018), URL: <http://elk.sourceforge.net/>.
- [19] J.P. Perdew, A. Ruzsinszky, G.I. Csonka, O.A. Vydrov, G.E. Scuseria, L.A. Constantin, X. Zhou, K. Burke, Phys. Rev. Lett. 100 (2008) 136406, , <https://doi.org/10.1103/PhysRevLett.100.136406>.
- [20] M. Kawamura, Comput. Phys. Commun 239 (2019) 197–203, <https://doi.org/10.1016/j.cpc.2019.01.017> ISSN 0010-4655.
- [21] T. Mizokawa, A. Fujimori, Phys. Rev. B 54 (1996) 5368, <https://doi.org/10.1103/PhysRevB.54.5368>.
- [22] H. Kawano, H. Yoshizawa, Y. Ueda, J. Phys. Soc. Jpn 63 (1994), <https://doi.org/10.1143/JPSJ.63.2857>.
- [23] T. Qian, N. Xu, Y.-B. Shi, K. Nakayama, P. Richard, T. Kawahara, T. Sato, T. Takahashi, M. Neupane, Y.-M. Xu, et al., Phys. Rev. B 83 (2011) 140513, , <https://doi.org/10.1103/PhysRevB.83.140513>.
- [24] K. Hashimoto, M. Yamashita, S. Kasahara, Y. Senshu, N. Nakata, S. Tonegawa, K. Ikada, A. Serafin, A. Carrington, T. Terashima, et al., Phys. Rev. B 81 (2010) 220501, , <https://doi.org/10.1103/PhysRevB.81.220501>.
- [25] J.K. Dong, S.Y. Zhou, T.Y. Guan, H. Zhang, Y.F. Dai, X. Qiu, X.F. Wang, Y. He, X.H. Chen, S.Y. Li, Phys. Rev. Lett. 104 (2010) 087005, , <https://doi.org/10.1103/PhysRevLett.104.087005>.
- [26] J.D. Fletcher, A. Serafin, L. Malone, J.G. Analytis, J.-H. Chu, A.S. Erickson, I.R. Fisher, A. Carrington, Phys. Rev. Lett. 102 (2009) 147001, , <https://doi.org/10.1103/PhysRevLett.102.147001>.
- [27] M. Yamashita, Y. Senshu, T. Shibauchi, S. Kasahara, K. Hashimoto, D. Watanabe, H. Ikeda, T. Terashima, I. Vekhter, A.B. Vorontsov, et al. Phys. Rev. B 84 (2011) 060507, , <https://doi.org/10.1103/PhysRevB.84.060507>.
- [28] Y. Zhang, Z.R. Ye, Q.Q. Ge, F. Chen, J. Jiang, M.B. Xu, P. Xie, D.L. Feng, Nature Phys. 8 (2012) 371–375.
- [29] X. Qiu, S.Y. Zhou, H. Zhang, B.Y. Pan, X.C. Hong, Y.F. Dai, M.J. Eom, J.S. Kim, Z.R. Ye, Y. Zhang, Phys. Rev. X 2 (2012) 011010, , <https://doi.org/10.1103/PhysRevX.2.011010>.
- [30] Z.-R. Ye, Y. Zhang, B.-P. Xie, D.-L. Feng, Chin. Phys. B 22 (2013) 087407URL: <https://doi.org/10.1088%2F1361-648x%2Faaf7e0>.
- [31] Z. Guguchia, A. Amato, J. Kang, H. Luetkens, P. Biswas, G. Prando, F. von Rohr, Z. Bukowski, A. Shengelaya, H. Keller, et al., Nat. Commun. 6 (2015) 8863.
- [32] F. Wang, H. Zhai, D.-H. Lee, Phys. Rev. B 81 (2010) 184512, , <https://doi.org/10.1103/PhysRevB.81.184512>.
- [33] K. Suzuki, H. Usui, K. Kuroki, J. Phys. Soc. Jpn 80 (2011) 013710, , <https://doi.org/10.1143/JPSJ.80.013710>.
- [34] E. Hassinger, P. Bourgeois-Hope, H. Taniguchi, S. René de Cotret, G. Grissonnanche, M.S. Anwar, Y. Maeno, N. Doiron-Leyraud, L. Taillefer, Phys. Rev. X 7 7 (2017) 011032, , <https://doi.org/10.1103/PhysRevX.7.011032>.